

### Accepted Manuscript



This is an *Accepted Manuscript*, which has been through the Royal Society of Chemistry peer review process and has been accepted for publication.

Accepted Manuscripts are published online shortly after acceptance, before technical editing, formatting and proof reading. Using this free service, authors can make their results available to the community, in citable form, before we publish the edited article. We will replace this Accepted Manuscript with the edited and formatted Advance Article as soon as it is available.

You can find more information about *Accepted Manuscripts* in the **Information for Authors**.

Please note that technical editing may introduce minor changes to the text and/or graphics, which may alter content. The journal's standard <u>Terms & Conditions</u> and the <u>Ethical guidelines</u> still apply. In no event shall the Royal Society of Chemistry be held responsible for any errors or omissions in this *Accepted Manuscript* or any consequences arising from the use of any information it contains.



## Toward In-Silico Modeling of Palladium-Hydrogen-Carbon Nanohorn Nanocomposites

Piotr Kowalczyk<sup>\*1</sup>, Artur P. Terzyk<sup>2</sup>, Piotr A. Gauden<sup>2</sup>, Sylwester Furmaniak<sup>2</sup> and Katsumi Kaneko<sup>3</sup>

[1] Nanochemistry Research Institute, Department of Chemistry, Curtin University of Technology, P.O. Box U1987, Perth, 6845 Western Australia, Australia

[2] Department of Chemistry, Physicochemistry of Carbon Materials Research Group, N. Copernicus University, Gagarin St. 7, 87-100 Torun, Poland

[3] Center for Energy and Environmental Science, Shinshu University, 4-17-1 Wakasato, Nagano 380-8553, Japan

Corresponding author footnote (\*To whom correspondence should be addressed):

#### Dr Piotr Kowalczyk

Tel: +61 8 9266 7800

E-mail: <u>Piotr.Kowalczyk@curtin.edu.au</u>

#### **Abstract**

We present the first *in-silico* modeling of the Pd-H-single-walled carbon nanohorn nanocomposites. Temperature-quench Monte Carlo simulations are used to generate the most stable morphologies of Pd<sub>81</sub> clusters (cluster sizes of ~2 nm) deposited inside the morphologically defective single-walled carbon nanohorns (S. Furmaniak, A. P. Terzyk, K. Kaneko, P. A. Gauden, P. Kowalczyk, T. Itoh, *Phys. Chem. Chem. Phys.*, 2013, **15**, 1232-1240). The optimized Pd<sub>81</sub>-single-walled carbon nanohorn nanocomposites are next used in calculating the H binding energy distributions at 300 K. The most stable positions of H impurity in confined Pd<sub>81</sub> clusters are identified, showing subsurface character of H absorption from the dilute H<sub>2</sub> gas at 300 K. The H binding energy distribution on Pd(100) open surface at 300 K is computed and compared with those corresponding to Pd<sub>81</sub>-single-walled carbon nanohorn nanocomposites. Finally, the impact of the Pd-H short-range order on the H binding energy is explored and critically discussed.

**Keywords**: metal-carbon nanocomposites, Pd clusters, carbon nanohorns, embedded atom method, Monte Carlo simulation.

#### I. Introduction

The possibility of fabricating and controlling the structure of metallic clusters and alloys inside ordered carbon-based materials (e.g. single-walled carbon nanohorns, single-walled carbon nanotubes, ordered porous carbons, stacked-cup carbon nanofibers, double-walled carbon nanotubes, bamboo-type multi-walled carbon nanotubes, etc.) is one of the challenges of catalytic science and technology<sup>1-7</sup>. From the practical point of view, nano-scale clusters and alloys deposited in carbonaceous nanopores may exhibit interesting catalytic properties, such as shape-selective catalysis, high catalytic activity near ambient temperatures, enhanced resistance towards sintering and deterioration, high hydrogen storage capacity, and fast kinetic of hydrogen loading/unloading<sup>1-7</sup>. From a fundamental perspective, the morphology, stability and reactivity of nanometer-sized metallic clusters and alloys deposited inside carbonaceous nanopores are still poorly understood.

Single-walled carbon nanohorns (SWCNHs) belong to a class of carbon nanomaterials consisting of single-walled carbon nanotubes (with diameter of 2-5 nm and a length of 20-50 nm) terminated with horn-shaped tips (having a conical angle of 20°)<sup>8-10</sup>. Individual carbon nanohorns self-assemble to form roughly spherical dahlia flower-like aggregates of 80 nm diameter. SWCNHs aggregates produced by CO<sub>2</sub> laser ablation of a graphitic rod in Ar have closed internal nanopores<sup>8-10</sup>. However, it has been shown that the controlled process of heating in O<sub>2</sub> at 693 K can easily open the internal SWCNHs pore spaces<sup>11</sup>. Therefore, the high capacity tubular and conical carbon nano-spaces can be accessible to guest particles, including metallic clusters and alloys. The sizes of nano-windows in SWCNHs are controlled by the length of O<sub>2</sub> oxidation, allowing adjustment of the molecular sieving properties<sup>12</sup>. The previous works of Kaneko and co-workers on the deposition of Pd nanoclusters in SWCNHs aggregates have shown an increased catalytic activity and hydrogen storage capacity of Pd-tailored SWCNH nanocomposites<sup>6,7</sup>. Bekyarova et al. argued that Pd-clusters deposited on SWCNHs have a significant contribution to the observed enhancement of H<sub>2</sub> storage in Pd-SWCNH nanocomposites at 303 K<sup>6</sup>. The steep uptake of H<sub>2</sub> adsorption measured at low H<sub>2</sub> pressures indicates strong interactions between H<sub>2</sub> and confined Pd nanoclusters. It is argued that H<sub>2</sub> molecules are decomposed to H atoms on confined Pd clusters, followed by formation of Pd-H alloys inside SWCNHs. Itoh et al. reported the high catalytic activity of Pd-SWCNH nanocomposites toward water

formation reaction at 273 and 298 K<sup>7</sup>. While these experimental results have revealed a great potential of Pd-tailored SWCNH nanocomposites in catalysis and H<sub>2</sub> storage, our understanding of these processes at an atomistic level is still largely incomplete. Indeed, the full atomistic simulations of the Pd-SWCNH nanocomposites have been hampered by the complexity of these systems. Moreover, extensive studies of these systems (i.e., 100-300 Pd and 1000-3000 carbon atoms) by simulations at the *ab initio* level are computationally prohibitive.

This work presents the first attempt to model Pd-SWCNH and Pd-H-SWCNH nanocomposites by fully atomistic molecular simulations. We wish to answer the following questions: What is the most stable morphology of Pd clusters deposited inside SWCNHs? What is the average and dispersion of H binding energy on Pd-SWCNH nanocomposites? How does nano-scale confinement stabilize Pd and Pd-H clusters? To answer these questions, we investigated three representative samples of  $Pd_{81}$ -SWCNH nanocomposites. The sizes of deposited Pd clusters of  $\sim 2$  nm and the atomistic structures of SWCNHs are consistent with the recent high-resolution transmission electron micrograph (HR-TEM) observations<sup>6,7</sup>. To model Pd<sub>81</sub> cluster deposition inside SWCNHs and the binding of H on Pd<sub>81</sub>-SWCNH nanocomposites we developed state-of-the-art Monte Carlo simulation methods implemented with density functional theory-based many-body potentials. Description of theory and simulation methodology is presented in section II. In section III, we present the final results and discussion with special attention to the relation between the Pd-H shortrange order and the strength of the H binding on Pd<sub>81</sub>-SWCNH nanocomposites. The conclusions are summarized in section IV.

#### II. Theory and Simulation Methodology

#### **II.1. Potential Models**

The nanocomposites studied consist of Pd and Pd-H clusters confined in internal nano-spaces of SWCNHs. To model these complex metal-carbon nanocomposites, appropriative all-atom potential models should be applied. For description of C-C interactions we use the environmental-dependent interaction potential (EDIP) developed by Marks<sup>13,14</sup>. The embedded-atom method (EAM) of Zhou *et* al.<sup>15</sup> is employed for performing potential energy calculations in confined Pd

and Pd-H clusters. The DFT-based Morse potential of Cheng and Lan<sup>16</sup> is used to compute the potential energy between Pd and C atoms. The functional forms of these potentials are presented below. For complete descriptions and other details, please refer to the original articles<sup>13-16</sup>.

Correct description of the interactions between carbon atoms is a challenging problem due to the mixed hybridization of C-C bonds in carbonaceous materials. The functional form of the EDIP potential therefore consists of three components: two-body pair energy, a three-body angular penalty, and a generalized coordination<sup>13,14</sup>. Following Marks, the total potential energy is written as a sum of no-site energies<sup>13,14</sup>:

$$U_{C-C} = \sum_{j} U_2(r_{ij}, Z_i) + \sum_{j < k} U_3(r_{ij}, r_{ik}, \theta_{jik}, Z_i)$$
(1)

where the pair potential  $U_2$  and the three-body term  $U_3$  in EDIP are parameterized using high quality *ab initio* data<sup>13,14</sup>. It is worth noting that the EDIP potential has been successfully used for modeling of the atomistic structure of various carbonaceous materials, including SWCNHs<sup>17-23</sup>. The functional forms of two- and three-body terms in Eq.1 and the accompanying set of parameters are given elsewhere<sup>13,14</sup>.

The many-body interactions in Pd and Pd-H clusters confined in SWCNHs are computed from the EAM developed by Zhou et al. 15. The total potential energy of a system consisting of N atoms (e.g., Pd and H) in EAM is given by the following functional form 15:

$$U_{Pd/H} = \frac{1}{N} \left[ \sum_{i=1}^{N} F_i(\rho_i) + \frac{1}{2} \sum_{i=1}^{N} \sum_{\substack{j=1 \ j \neq i}}^{N} \phi_{ij}(r_{ij}) \right]$$
(2)

where  $F_i(\rho_i)$  is an embedding energy at the site of atom i with a background electron density of  $\rho_i$ , and  $\phi_{ij}(r_{ij})$  is a pair energy between atoms i and j separated by a distance  $r_{ij}$ . Electron density at the site of atom i is calculated from 15:

Page 6 of 22

$$\rho_i = \sum_{\substack{j=1\\j\neq i}}^N \rho_j^a \left( r_{ij} \right) \tag{3}$$

were  $\rho_j^a(r_{ij})$  is the electron density contribution from atom j that is  $r_{ij}$  away from site i. The EAM potential given by Eq. 2 requires three functions for each element (e.g., i = Pd, H): the embedding energy  $F_i(\rho_i)$  as a function of electron density  $\rho$ ; the pair energy  $\phi_{ii}(r)$  as a function of atom distance r; and the atomic electron density  $\rho_i^a(r)$  as a function of atom distance r. In addition to these three functions for each of the elements, the cross-pair energy terms between dissimilar species i and j,  $\phi_{ij}(r)$ , is required for the Pd-H system. The analytical formulas for all these functions can be found in the original work of Zhou and co-workers<sup>15</sup>. It is worth noting, that opposed to other EAM potentials, the parameters in all these functions depend on the concentration of H atoms in Pd<sup>15</sup>. As shown by Ruda et al.  $^{24,25}$ , the EAM potential of Zhou et al. correctly describes the H absorption in Pd clusters of various morphologies and Pd open surfaces.

We compute the Pd-C potential energy from the DFT-Morse potential of Cheng and Lan<sup>16</sup>:

$$U_{Pd-C}(r) = U_0 \left\{ \left[ 1 - \exp(-k(r - r_0)) \right]^2 - 1 \right\}$$
 (4)

where  $U_0 = 0.1132$  eV, k = 1.56 and  $r_0 = 2.73$  Å. As has been previously shown<sup>16</sup>, the first-principle Morse-type carbon-metal interaction potential is much stronger than those computed from the typical weak van der Waals Lennard-Jones potential model.

#### **II.2. Simulation Details and Computed Properties**

#### II.2.1. Pd<sub>81</sub> Clusters Inside Single-Walled Carbon Nanohorns

The atomistic structures of morphologically defective SWCNHs are taken from our previous work<sup>26</sup>. Face-centered cubic (fcc) Pd crystal containing 81 atoms was deposited inside three samples of SWCNHs (i.e., NH\_1.71\_03.0\_19.2,

NH\_2.33\_03.0\_19.2 and NH\_2.66\_03.0\_19.2, see Figure 1 (b) in reference 26 and Figure 1S in ESI). The following notation was used<sup>26</sup>: NH\_ddd\_lll\_aaa, where ddd, lll, and aaa are the diameter of tubular part (in nm), the length of tubular part (in nm), and the apex angle (in grades). Note that selected samples of SWNHs have progressively increasing diameter of the tubular part (i.e., 1.71, 2.33 and 2.64 nm, respectively) whereas the apex angle of the conical part of 19.2° is fixed<sup>26</sup>. For each SWCNH sample, we generate twelve initial configurations of fcc-Pd<sub>81</sub> crystal inside SWCNH by randomly placing its center of mass into the tubular part. Then, we optimize the structures of Pd<sub>81</sub>-SWCNH nanocomposites using in silico temperature-quench Monte Carlo simulations implemented in NVT ensemble<sup>27</sup> (see Figure 1 and movie movie\_1.mpg in ESI). As previously, the temperature decreases linearly from 3000 K down to 300 K, with a step of 10 K<sup>26</sup>. For each temperature, 100 Monte Carlo perturbations (including random displacement of Pd and C atom) were performed using the Metropolis algorithm<sup>28</sup>. The displacement of Pd and C atoms is adjusted every 1000 Monte Carlo steps to maintain the acceptance ratio of 0.4.

#### II.2.2. Pd<sub>81</sub>-H Clusters Inside Single-Walled Carbon Nanohorns

The optimized structures of  $Pd_{81}$ -SWNH nanocomposites were used for calculation of the H binding energy. An H atom was placed on the surface of the confined  $Pd_{81}$  cluster at a random position, followed by the relaxation of the  $Pd_{81}$ -H-SWCNH nanocomposite in NVT ensemble by the Monte Carlo method at 300 K (see movie\_2,mpg in ESI). At least 120 random positions of H atoms were generated for each  $Pd_{81}$ -SWCNH nanocomposite. We performed  $10^6$  Monte Carlo steps; each step consists of attempting moves of the randomly selected Pd, H and C atoms. The Metropolis criterion<sup>28</sup> was used to accept the displacement perturbation. The acceptance ratio was set to be approximately 0.4.

#### II.2.3. H Binding Energy on Pd<sub>81</sub>-SWCNH Nanocomposites

The binding energy of H on  $Pd_{81}$ -SWCNH nanocomposites at 300 K was calculated using the following expression<sup>29</sup>:

$$E_b = E_{total} \left( Pd_{81} - SWCNH - H \right) - E_{total} \left( Pd_{81} - SWCNH \right) - \frac{1}{2} E_{total} \left( H_2 \right)$$
 (5)

where  $E_{total}(Pd_{81}-SWCNH-H)$  is the formation energy of the  $Pd_{81}$ -SWCNH-H nanocomposite,  $E_{total}(Pd_{81}-SWCNH)$  denotes the formation energy of  $Pd_{81}$ -SWCNH nanocomposite, and  $E_{total}(H_2)$  is the binding energy of hydrogen molecule. Negative  $E_b$  corresponds to the H atom dissolved in  $Pd_{81}$ -SWCNH being energetically stable with respect to free hydrogen molecules. Following Christensen et al.  $^{29}$ , in calculating the binding energies we neglected the contribution from zero-point energies. In all calculations, we used the experimental value of  $E_{total}(H_2) = 4.75 \text{ eV}^{30}$ .

The binding energy of H atom on  $Pd_{81}$ -SWCNHs at 300 K depends on the position of the H impurity as well as the relaxation of neighboring Pd atoms. We would like to underline that even Pd open surfaces are microscopically heterogeneous<sup>31</sup>. Therefore, for each studied  $Pd_{81}$ -SWCNH nanocomposite, we collected the histograms of  $E_b$  from Monte Carlo simulations in NVT ensemble at 300 K. For comparison, we computed the histogram of  $E_b$  for Pd(100) open surface. Next, we described each histogram by the mathematical function that takes into account the asymmetry factor<sup>18</sup>:

$$P(E_{b}) = \begin{cases} 0, & \text{if } E_{b} < M - \frac{D(4 - a^{2})}{2a} \\ H \exp\left\{\left(\frac{4}{a^{2}} - 1\right) \left[\ln\left(1 + \frac{2a(E_{b} - M)}{D(4 - a^{2})}\right) - \frac{2a(E_{b} - M)}{D(4 - a^{2})}\right]\right\}, & \text{elsewhere} \end{cases}$$
(6)

where  $P(E_b)$  denotes the probability distribution function, M is the peak maximum (i.e., the most probable value of  $E_b$ ), H>0 denotes peak height, 0 < a < 2 is the asymmetry factor and D>0 is the standard deviation. Note that for  $a \to 0$ , Eq. 6 is reduced to the symmetrical Gaussian distribution  $^{18}$ .

#### II.2.4. Pd-H Short-Range Order

The relaxation and ordering of Pd atoms around the H impurity may shed some light into the relation between the Pd-H short-range order and the strength of the H binding. To characterize the local order of Pd atoms around H impurity we collected radial histograms from the NVT Monte Carlo simulations at 300 K<sup>27</sup>. Spherical shells with specified pore radius were built around the H impurity. During NVT Monte Carlo run, we measured the distance between the H impurity and each Pd atom. The calculations of radial histograms are performed for selected positions of the H impurity. For each collected radial histogram at least 10<sup>5</sup> Monte Carlo configurations are analyzed.

#### III. Results and Discussion

Pd (and other metal) nanoclusters are unstable in air because their fast growth is induced by coalescence<sup>32</sup>. Pd nanoclusters can however, be stabilized by their confinement in nano-scale pores of SWCNHs (see Kaneko et al.<sup>6,7</sup>). The most probable positions and morphology of Pd clusters deposited in SWNHs are difficult to access by direct experimental observations. We should also keep in mind that processes accompanying deposition of Pd clusters in SWCNHs are out of thermodynamic equilibrium. Therefore, one can expect the formation of Pd clusters on both internal and external surface of SWCNHs. The size and morphology of these Pd clusters can be different, depending on the synthesis conditions and the place of deposition. Indeed, high-resolution transmission electron microscopic images (HRTEM) show that Pd clusters of approximately 2-3 nm diameters are highly dispersed on the external and internal surface of oxidized SWCNHs<sup>6,7</sup>. Furthermore, Pd clusters filling the horn-shaped tips of SWCNHs are clearly visible in the highly magnified HRTEM images<sup>7</sup> (see top panel in Figure 2). Similarly, Iijima and coworkers reported preferential deposition of Gd<sub>2</sub>O<sub>3</sub> nanoparticles of about 2.3 nm in average diameter inside horn-shaped tips<sup>1,4</sup>. The authors concluded that the deep potential fields of the SWCNH nanospaces confined the Gd-acetate and its thermal derivatives, thus preventing the sublimation and the migration to coalesce to larger particles. Our temperature-quench Monte Carlo simulations show that the most probable position of Pd81 clusters confined in SWCNHs are indeed within hornshaped tips (see bottom panel in Figure 2). We notice that melted fcc-Pd<sub>81</sub> crystals are strongly attracted by the curved carbon surface of conical tips, showing fast rate of cluster deposition (see Figure 1 and movie\_1.mpg in ESI). This observation is not unexpected because the enhanced Pd-C potential (i.e., surface forces) inside conical tips drags the Pd<sub>81</sub> clusters from the tubular to the conical part. As a result, Pd<sub>81</sub> clusters deposited inside SWCNHs resemble the conical shape of tips (see Figures 1-2). Thus, we conclude that the apex angle of horn-shaped tips of SWCNHs controls the morphology of confined Pd clusters in the absence of kinetic traps (e.g. defects, heteroatoms, impurities, surface functional groups, etc.). This finding can be particularly important for tuning catalytic reactivity and the electronic properties of Pd-SWNCH nanocomposites (such as reaction barrier for catalytic reactions and electronic band structures), however, detailed study of these important research problems are beyond the scope of the current work.

Pd surfaces, including Pd open planes and curved surfaces of clusters, are structurally and energetically heterogeneous. Intrinsic disorder of Pd atoms close to the surface implies that the binding energy of the H atom is position dependent. Strictly speaking, the local ordering and relaxation of Pd atoms around an H impurity is not unique but is varies locally along the heterogonous surface. Indeed, the binding energy of H atom on Pd(100) and Pd<sub>81</sub>-SWCNH nanocomposites has a typical Gaussian bell-shape (see Table 1 and Figure 3). However, in strict contrast to the Pd(100) open surface, the H binding energy distributions computed for Pd<sub>81</sub> clusters confined in SWNHs are more homogenous and shifted to lower values of binding energy. The shift of 0.4-0.6 eV/atom (i.e., 36-58 kJ/mol) can be explained by the fact that surface atoms in clusters are more reactive than surface atoms on the Pd(100) open surface. By forming Pd<sub>81</sub>-H composites, H impurity stabilizes Pd<sub>81</sub> clusters. Therefore, we speculate that the higher binding energy of H on confined Pd clusters is responsible for the enhanced H<sub>2</sub> storage measured experimentally for Pd-SWCNH nanocomposites at 303 K<sup>6</sup>. The observed homogeneity of H binding energy distributions computed for confined Pd<sub>81</sub> clusters results from the finite size effects. Simply, the number of Pd configurations around H impurity is significantly smaller for the Pd<sub>81</sub> clusters than for the Pd(100) open surface. Interestingly, the H binding energy distributions computed for confined Pd<sub>81</sub> clusters are similar for all studied SWCNHs samples (see Figure 3). This further indicates that the apex angle of conical tips that determines the morphology of deposited Pd<sub>81</sub> clusters also has an impact on

the binding energy of H at infinite dilution of H<sub>2</sub> gas at 300 K. Notice that Pd clusters deposited on oxidized samples of SWNCHs have a range of sizes. Thus, for the fixed apex angle of conical tips, the observed catalytic reactivity of Pd-SWNCH nanocomposites may strongly depend on the size distribution of the deposited Pd clusters. Furthermore, reproducibility of the experimental measurements of the catalytic activities can be achieved by tuning the Pd cluster size distributions inside SWCNHs, which is an experimental challenge.

Figure 4 presents microscopic snapshots of H-Pd<sub>81</sub> configurations in the NH 1.71 03.0 19.2 nanohorn. The preferential absorption site for the H impurity is a subsurface. We found that H atoms randomly placed at the surface of confined Pd<sub>81</sub> clusters quickly diffuse to the regions of subsurface. This feature of H absorption in Pd has been observed for various Pd clusters and Pd open surfaces<sup>24,25</sup>. Thus, the subsurface absorption of H on Pd does not result from the specific morphology of Pd<sub>81</sub> clusters deposited in SWCNHs, but it is rather connected with the electronic properties of Pd atoms. The remaining question to answer is how the local ordering and relaxation of Pd atoms around H impurity impact the binding energy? Radial histograms of Pd atoms around H impurity highlight the relationship between the Pd-H short-range order and the binding energy (see Figure 5). Higher number of Pd atoms in the contact layer as well as layered structures of Pd atoms around the H impurity result in lower binding energy (i.e., 4.16 and 4.31 eV/atom in Figure 5). Disorder of the local structure of Pd atoms around H impurity alters the H binding energy by approximately 0.8-1.0 eV/atom (i.e., 77-96 kJ/mol). The most probable binding energy of H on Pd<sub>81</sub>-SWCNH nanocomposites is around 3.7-3.8 eV/atoms (see Table 1 and Figure 3), indicating short-range ordering of Pd atoms around H impurity.

#### **IV. Conclusions**

Deposition of Pd clusters on oxidized samples of SWCNHs, H<sub>2</sub> storage close to ambient temperatures, and catalytic activities of confined Pd clusters are complex research problems. The morphologies and sizes of deposited Pd clusters are strongly dependent on the synthesis conditions. This makes the interpretation of the experimental data measured for composite metal-organic materials very difficult.

In this study we have developed computational methodology for the *in-silico* modeling of the Pd-H-single-walled carbon nanohorn nanocomposites. The first sets of temperature-quench Monte Carlo simulations are carried out to predict the most stable morphologies of Pd<sub>81</sub> clusters inside morphologically defective single-walled carbon nanohorns. We observed that all simulated Pd<sub>81</sub> clusters are preferentially deposited inside the conical tips of carbon nanohorns. This finding can be explained by the action of the enhanced surface forces in conical tips and the lack of kinetic barriers in our computer experiments. Interestingly, high-resolution transmission electron micrograph images of Pd clusters inside oxidized SWCNHs show that Pd clusters fill conical carbon tips. Therefore, either in real or model SWCNHs, the shape of carbon tips determines the morphology of confined Pd clusters.

The next set of simulations was carried out to evaluate the H binding energy on optimized Pd-SWCNH nanocomposites at 300 K. We find that H binding energy distributions computed for Pd81-SWCNH nanocomposites are more homogenous and shifted to lower values of binding energy as compared to a Pd(100) open surface. A shift of H binding energy of ~0.4-0.6 eV/atom (i.e., 36-58 kJ/mol) is expected because Pd<sub>81</sub> clusters are more reactive than Pd(100) open surface. Therefore, we conclude that small Pd nanoclusters stabilized inside oxidized SWCNHs are responsible for the enhanced H<sub>2</sub> storage at 303 K observed experimentally<sup>6</sup>. Microscopic snapshots collected from molecular simulations clearly show that the H binding energy is correlated with the Pd-H short-range order. High binding energies of H on Pd<sub>81</sub>-SWCNH nanocomposites (of ~4.1-4.3 eV/atom) are observed for ordered Pd structures around a H impurity at short H-Pd distances. Disorder of Pd atoms around H impurity alters the H binding energy by approximately 0.8-1.0 eV/atom (i.e., 77-96 kJ/mol). Further insight into the relation between the Pd cluster size, H binding energy and the morphology of single-walled carbon nanotubes are currently under study.

#### Acknowledgements

P.K. acknowledges partial support by the Office of Research & Development, Curtin University, Grant CRF10084. P.K. acknowledges partial support by the Japanese Society for Promotion of Science (short-term JSPS Invitation Fellowship). K.K. was supported by Exotic Nanocarbons, Japan Regional Innovation Strategy Program by

the Excellence, JST. The authors acknowledge Professors Julian Gale (Curtin University) and Leslie Glasser (Curtin University) for fruitful comments and discussions connected with this research work. APT, PAG, and SF acknowledge the use of the computer cluster at Poznań Supercomputing and Networking Center and the Information and Communication Technology Center of the Nicolaus Copernicus University (Toruń, Poland).

Electronic supplementary information (ESI) available: Movie\_1: The optimization of structures of Pd<sub>81</sub>-SWCNH nanocomposites (NH\_2.33\_03.0\_19.2 and NH\_2.66\_03.0\_19.2 nanohorn samples) using *in silico* temperature-quench Monte Carlo simulations implemented in NVT ensemble. Movie\_2: The relaxation of four representative samples of Pd<sub>81</sub>-H-SWCNH nanocomposite in NVT ensemble by the Monte Carlo method at 300 K. Figure 1S: Snapshots of Pd<sub>81</sub>-SWCNH nanocomposites (NH\_1.71\_03.0\_19.2, NH\_2.33\_03.0\_19.2 and NH\_2.64\_03.0\_19.2 nanohorn samples) collected from temperature-quenched Monte Carlo simulations. Figure 1, 2, 4 and 1S and all movies were created using Visual Molecular Dynamics (VMD) program<sup>33</sup>.

#### References

- (1) A. Hashimoto, H. Yorimitsu, K. Ajima, K. Suenaga, H. Isobe, J. Miyawaki, M. Yudasaka, S. Iijima, E. Nakamura, *Proc. Natl. Acad. Sci. USA*, 2004, **101**, 8527-8530.
- (2) P. M. Ajayan, S. Iijima, *Nature*, 1993, **361**, 333-334.
- (3) G. G. Wildgoose, C. E. Banks, R. G. Compton, *Small*, 2006, **2**, 182-193.
- (4) J. Miyawaki, M. Yudasaka, H. Imai, H. Yorimitsu, H. Isobe, E. Nakamura, S. Iijima, *J. Phys. Chm. B*, 2006, **110**, 5179-5181.
- (5) R. Kitaura, N. Imazu, K. Kobayashi, H. Shinohara, Nano. Lett., 2008, 8, 693-699.
- (6) E. Bekyarova, A. Hashimoto, M. Yudasaka, Y. Hattori, K. Murata, H. Kanoh, D. Kasuya, S. Iijima, K. Kaneko, *J. Phys. Chem. B.*, 2005, **109**, 3711-3714.
- (7) T. Itoh, K. Urita, E. Bekyarova, M. Arai, M. Yudasaka, S. Iijima, T. Ohba, K. Kaneko, H. Kanoh, *J. Coll. Int. Sci.*, 2008, **322**, 209-214.
- (8) S. Iijima, M. Yudasaka, R. Yamada, S. Bandow, K. Suenaga, F. Kokai, K.

- Takahashi, Chem. Phys. Lett., 1999, 309, 165-170.
- (9) P. Kowalczyk, R. Holyst, H. Tanaka, K. Kaneko, *J. Phys. Chem. B*, 2005, **109**, 14659-14666.
- (10) L. Hawelek, A. Brodka, J. C. Dore, A. C. Hannon, S. Iijima, M. Yudasaka, T. Ohba, K. Kaneko, A. Burian, *J. Phys. Chem. A*, 2013, **117**, 9057-9061.
- (11) E. Bekyarova, K. Kaneko, M. Yudasaka, D. Kasuya, S. Iijima, A. Huidobro, F. Rodriguez-Reinoso, *J. Phys. Chem. B*, 2003, **107**, 4479-4484.
- (12) K. Murata, K. Hirahara, M. Yudasaka, S. Iijima, D. Kasuya, K. Kaneko, *J. Phys. Chem. B*, 2002, **106**, 12668-12669.
- (13) N. A. Marks, Phys. Rev. B, 2000, 63, 035401-035408.
- (14) N. A. Marks, *Phys. Rev. B*, 1997, **56**, 2441-2446.
- (15) X. W. Zhou, J. A. Zimmerman, B. M. Wong, J. J. Hoyt, *J. Mat. Res.*, 2008, **23**, 704-718.
- (16) D. Cheng, J. Lan, Mol. Simul., 2010, 36, 805-814.
- (17) I. Suarez-Martinez, P. J. Higginbottom, N. A. Marks, *Carbon*, 2010, **48**, 3592-3598.
- (18) P. Kowalczyk, P. A. Gauden, A. P. Terzyk, RSC Adv., 2012, 2, 4292-4298.
- (19) S. Furmaniak, A. P. Terzyk, P. Kowalczyk, K. Kaneko, P. A. Gauden, *Phys. Chem. Chem. Phys.*, 2013, **15**, 16468-16476.
- (20) G. Opletal, T. C. Peterson, B. O'Malley, I. K. Snook, D. G. McCulloch, I. Yarovsky, *Comput. Phys. Commun.*, 2008, **178**, 777-787.
- (21) N. A. Marks, D. R. McKenzie, B. A. Pailthorpe, M. Bernasconi, M. Parrinello, Phys. Rev. B, 1996, 54, 9703-9714.
- (22) S. Furmaniak, A. P. Terzyk, K. Kaneko, P. A. Gauden, P. Kowalczyk, T. Ohba, *Chem. Phys. Lett.*, 2014, **595-596**, 67-72.
- (23) T. C. Peterson, I. K. Snook, I. Yarovsky, D. G. McCulloch, B. O'Malley, *J. Phys. Chem. C*, 2007, **111**, 802-812.
- (24) M. Ruda, E. A. Crespo, S. Ramos de Debiaggi, *J. Alloys and Comp.*, 2010, **495**, 471-475.
- (25) E. A. Crespo, M. Ruda, S. Ramos de Debiaggi, E. M. Bringa, F. U. Braschi, G. Bertolino, *Int. J. Hydrogen Energy*, 2012, **37**, 14831-14837.
- (26) S. Furmaniak, A. P. Terzyk, K. Kaneko, P. A. Gauden, Kowalczyk P., T. Itoh, *Phys. Chem. Chem. Phys.*, 2013, **15**, 1232-1240.

- (27) M. P. Allen, D. J. Tildesley, Computer Simulation of Liquids, Clarendon Press, Oxford, 1987.
- (28) N. Metropolis, A. W. Rosenbluth, M. N, Rosenblith, A. H. Teller, E. Teller, *J. Chem. Phys.*, 1953, **21**, 1087-1092.
- (29) O. B. Christensen, P. D. Ditlevsen, K. W. Jacobsen, P. Stoltze, O. H. Nielsen, J. K. Nørskov, Phys. Rev. B, 1989, 40, 1993(R).
- (30) O. M. Løvvik, R. A. Olsen, Phys. Rev. B, 1998, 58, 890-898.
- (31) W. Rudzinski, R. Charmas, S. Partyka, J. Y. Bottero, *Langmuir*, 1993, **9**, 2641-2651.
- (32) B. Corain, G. Schmid, N. Toshima (Editors), Metal Nanoclusters in Catalysis and Materials Science: The Issue of Size Control, Elsevier, Amsterdam, 2008.
- (33) W. Humphrey, A. Dalke, K. Schulten, J. Mol. Graphics, 1996, 14, 33-38.

Parameter	Sample			
	Pd(100)	NH_1.71_03.0_19.2	NH_2.33_03.0_19.2	NH_2.64_03.0_19.2
M, (eV/atom)	-3.27	-3.67	-3.73	-3.84
Н	0.48	1.45	1.27	0.94
а	0.05	0	0	0
D, (eV/atom)	0.85	0.27	0.31	0.39

**Table 1.** Parameters of hydrogen binding energy distributions (see Eq. 6) computed for Pd(100) open surface and three samples of Pd<sub>81</sub>-SWCNH nanocomposites. Abbreviations: M denotes the most probable value of hydrogen binding energy, H is peak height, a is the asymmetry factor and D denotes the standard deviation. Note that hydrogen binding energy distributions computed for confined Pd<sub>81</sub> clusters are more homogenous and shifted to higher values of binding energy as compared to Pd(100) open surface.

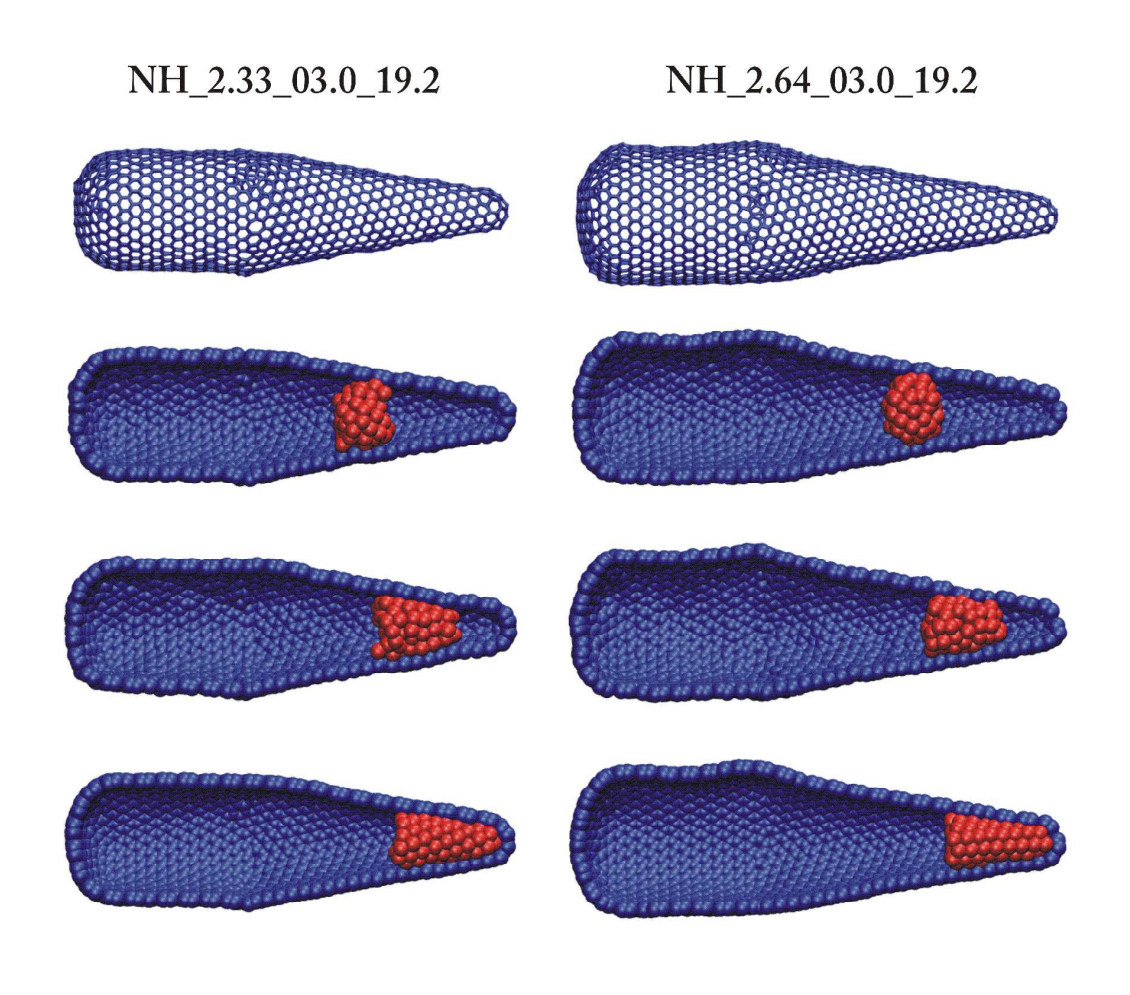


**Figure 1.** Snapshots of  $Pd_{81}$ -SWCNH nanocomposites (left panels: NH\_2.33\_03.0\_19.2 nanohorn, right panels: NH\_2.64\_03.0\_19.2 nanohorn) collected from temperature-quenched Monte Carlo simulations. Fcc-Pd<sub>81</sub> crystals confined in morphologically defective SWCNHs are melted at 3000 K (top panels), followed by the relaxation to the most stable morphologies at 300 K (bottom panels).

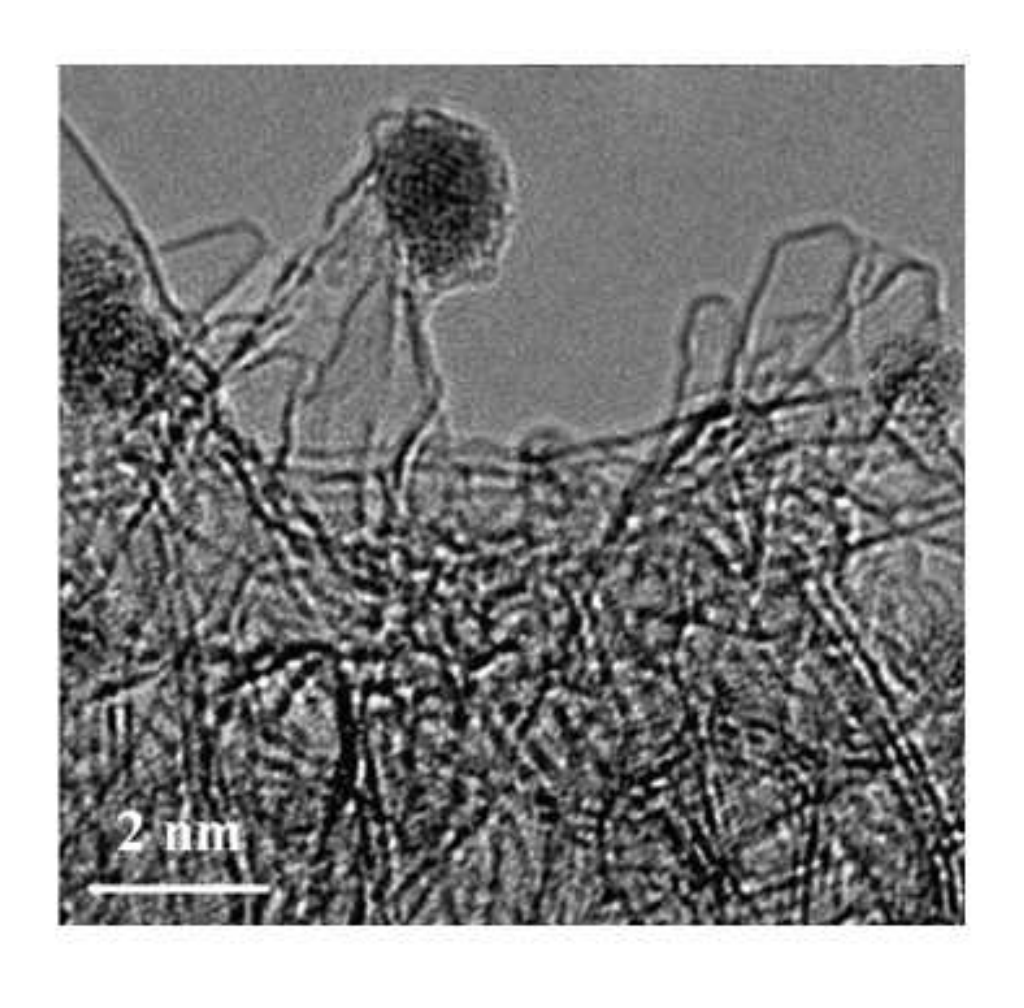




**Figure 2.** Top panel: High-resolution transmission electron micrograph (HRTEM) image of Pd clusters inside oxidized sample of SWCNHs at high magnification. Bottom panel: The optimized structure of  $Pd_{81}$ -SWCNH (NH\_2.64\_03.0\_19.2 nanohorn) nanocomposite generated from the temperature-quench Monte Carlo simulation. The sizes of confined  $Pd_{81}$  clusters studied by computer experiments are comparable with that observed in HRTEM.

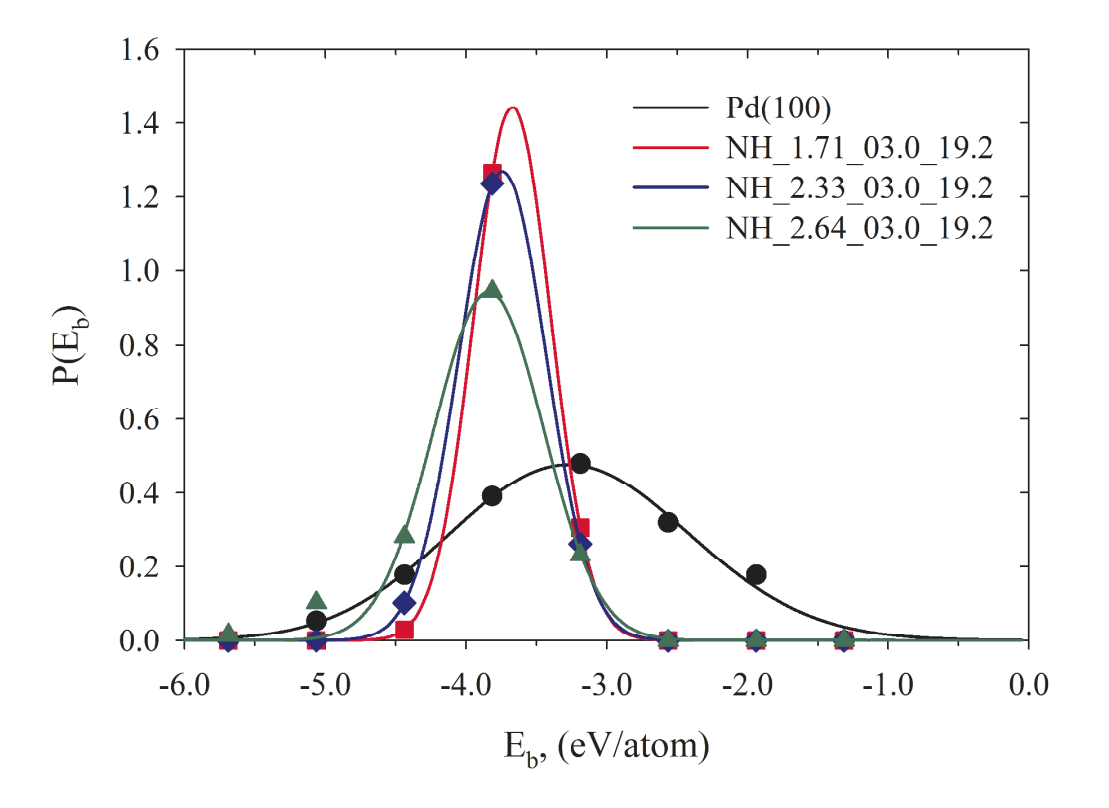


**Figure 3.** Distributions of H binding energy computed for three samples of  $Pd_{81}$ -SWCNH nanocomposites. For comparison, the H binding energy computed for Pd(100) open surface is presented. Close circles correspond to data collected from NVT Monte Carlo simulations at 300 K. Lines are generated by fitting Eq. 6 to simulation data (see Table 1).

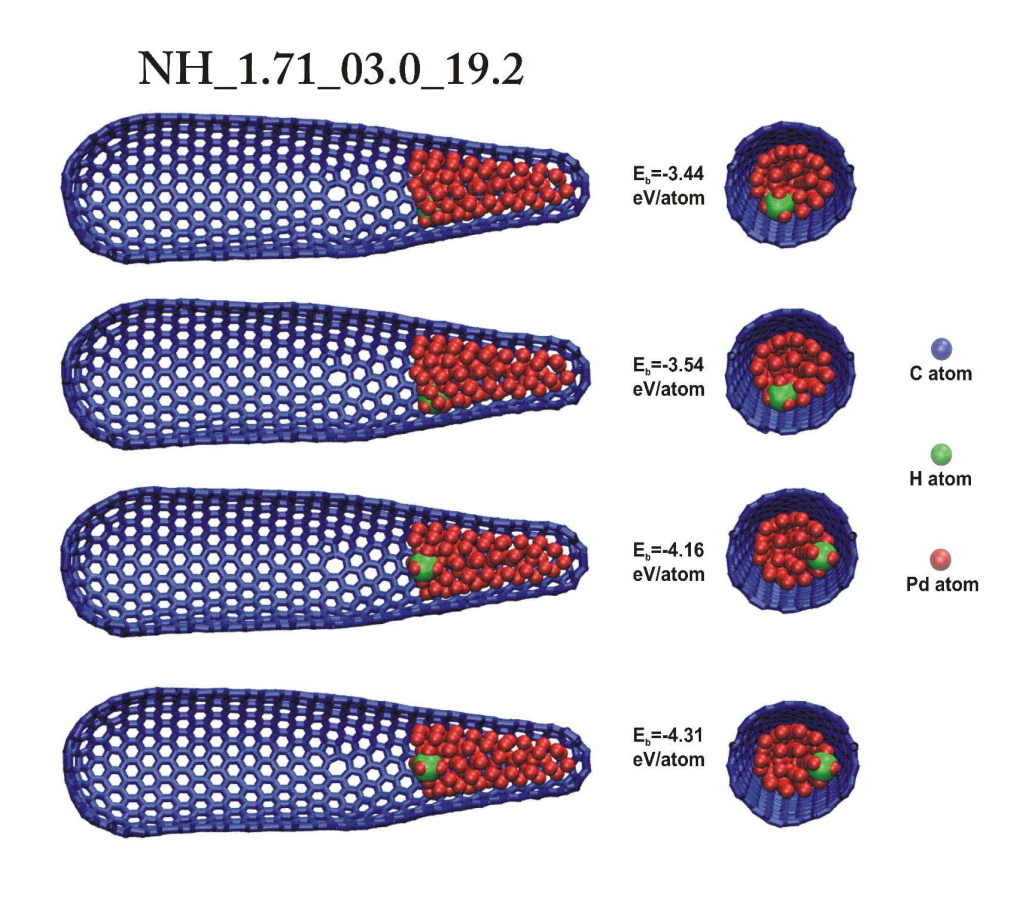


**Figure 4.** H-Pd<sub>81</sub>-SWCNH (NH\_1.71\_03.0\_19.2 nanohorn) nanocomposite snapshots collected from NVT Monte Carlo simulations at 300 K. The binding energies of H atom (green balls) computed from Eq. 5 are (from the top to the bottom): -3.44, -3.54, -4.16 and -4.31 eV/atom. The sizes of H atoms are magnified for clarity of the presentation. Note that subsurface is the preferential absorption site for H atoms. The Pd-H short-range order impacts the binding energy (see Figure 5 for more details).

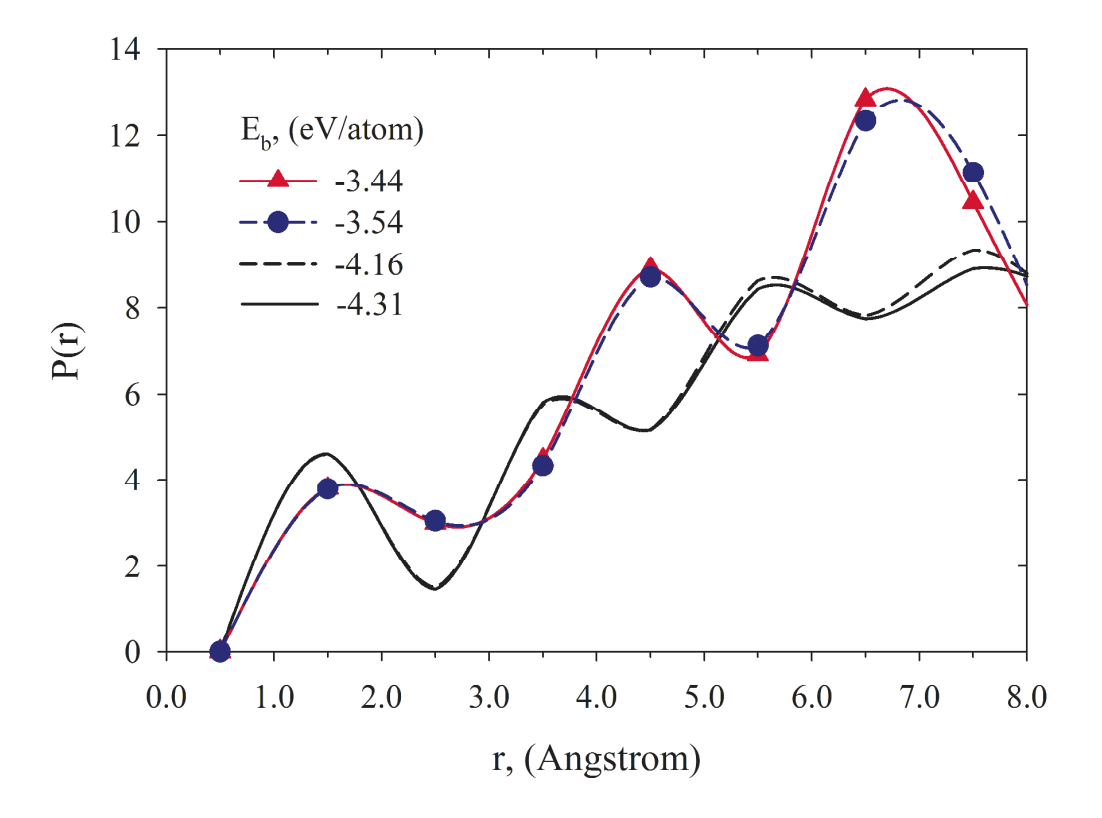
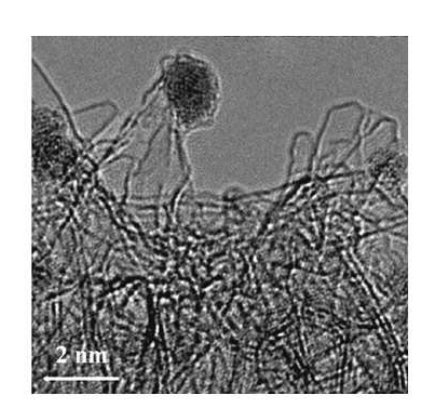


**Figure 5.** Radial histograms of Pd around H impurity collected in NVT Monte Carlo simulations at 300 K for NH\_1.71\_03.0\_19.2 nanohorn. The corresponding binding energies are given on the plot. Note that H impurity stabilizes the structure of Pd atoms. High values of H binding energies result from Pd-H short-range order (black lines). Disorder of Pd atoms around H impurity alters the binding energy (colored lines).



# In Silico Modeling of Pd-H-Carbon Nanohorn Nanocomposites



The first *in-silico* modeling of the Pd-H-single-walled carbon nanohorn nanocomposites show that apex angle of horn-shaped tips of single-walled carbon nanohorns controls the morphology and reactivity of confined Pd clusters.